Frontiers of Information Technology & Electronic Engineering
www.jzus.zju.edu.cn; engineering.cae.cn; www.springerlink.com
ISSN 2095-9184 (print); ISSN 2095-9230 (online)
E-mail: jzus@zju.edu.cn

Review:

Filtering antennas: from innovative concepts to industrial applications*

Yun-fei CAO, Yao ZHANG, Xiu-yin ZHANG†‡

School of Electronic and Information Engineering, South China University of Technology, Guangzhou 510641, China

†E-mail: zhangxiuyin@scut.edu.cn

Received Sept. 4, 2019; Revision accepted Jan. 14, 2020; Crosschecked Jan. 27, 2020

Abstract: A filtering antenna is a device with both filtering and radiating capabilities. It can be used to reduce the cross-band mutual coupling between the closely spaced elements operating at different frequency bands. We review the authors' work on filtering antenna designs and three related dual-band base-station antenna arrays as application examples. The filtering antenna designs include single- and dual-polarized filtering patch antennas, a single-polarized omni-directional filtering dipole antenna, and a dual-polarized filtering dipole antenna for the base station. The filtering antennas in this paper feature an innovative concept of eliminating extra filtering circuits, unlike other available antennas. For each design, the filtering structure is finely integrated with the radiators or feeding lines. As a result, the proposed designs have the advantages of compact size, simple structure, good in-band radiation performance, and low levels of loss, and do not contain complicated filtering circuits. Based on the proposed filtering antennas, single- and dual-polarized dual-band antenna arrays were developed. Separate antenna elements at different frequency bands were used to achieve the dual-band performance. The cross-band mutual couplings between the elements at different bands were reduced substantially using the antenna inherent filtering performance. The dual-band arrays exhibited better performance as compared to typical industrial products. Some of the proposed technologies have been transferred into the industry.

Key words: Filtering antenna; Dual-band; Antenna array
https://doi.org/10.1631/FITEE.1900474 **CLC number:** TN828.6

1 Introduction

A filtering antenna is a type of antenna which integrates the filtering functions into the antenna structure. In some cases, it can replace the cascading connection of the filter and antenna, avoid causing additional insertion loss, and achieve a more compact size, which is attractive when building multi-band arrays. Multi-band or multi-standard modern communication systems (e.g., 3G, 4G, and 5G), require multi-band base-station antenna arrays. The multi-band performance of the base-station antenna array is normally achieved using several separate subarrays operating at different frequencies. In this way, the radiation performances at different bands are very stable. However, there is serious interference between different subarrays at different bands due to the limited space of the antenna. Filtering antennas can be used in such cases to solve this problem due to their good out-of-band radiation suppression, which does not increase the total size of the multi-band array.

In the past, different methods for designing filtering antennas have been proposed. Among them, the most direct way is to connect the filtering circuits with the feeding line of the antenna radiators. Filtering antennas have been implemented using an antenna radiator as the last-stage resonator of the filter (Hsieh et al., 2015; Fakharian et al., 2016; Chen et al.,

‡ Corresponding author

* Project supported by the National Natural Science Foundation of China (Nos. 61725102 and 61701182) and the China Postdoctoral Science Foundation (Nos. 2017M610521 and 2018T110866)

ORCID: Yun-fei CAO, https://orcid.org/0000-0002-3282-7796; Xiu-yin ZHANG, https://orcid.org/0000-0001-9458-0074

2017; Hu et al., 2017; Tang et al., 2018). In Qin et al. (2015) and Deng et al. (2018), filtering antennas have been designed by integrating the filtering circuit into the feeding networks of the antennas. However, these designs still occupy a large space since they use multiple resonators. Additionally, the extra loss by the filtering circuits degrades the antenna gain.

Another method for designing filtering antennas is to deploy simple parasitic elements, which can extend the antenna operating bandwidth (Wu et al., 2013). In Sun et al. (2015), a parasitic strip was placed near the dipole radiator to improve its upper band-edge roll-off performance. Employing this technique, the operating bandwidth was improved to 27.5%. In Wu et al. (2015), a rectangular loop and parasitic strips were used to achieve lower and upper band-edge selectivities, respectively. The antenna has a passband bandwidth of 56.6%, with a flat gain. However, the mentioned antennas (Wu et al., 2013, 2015; Sun et al., 2015) have only a single polarization.

To solve the above-mentioned problems, we present several filtering antennas, including filtering patch and dipole antennas. The antennas use simple filtering circuits, and have the advantages of compact size, simple structure, and little extra loss of gain. Unlike in previous works, the in-band radiation performances of the proposed antennas are kept good, since the insertion loss of the filter is eliminated.

Regarding the industrial application of such antennas, three dual-band antenna array prototypes are introduced. In the dual-band arrays, mutual coupling between the elements operating at different bands is effectively suppressed using filtering antenna elements. This is done to reduce the spacing between the elements and obtain a compact antenna array. With these advantages, some of the proposed technologies have been applied in the base-station industry.

2 Compact filtering antennas without extra circuits

In this section, we review several proposed compact filtering antennas without extra circuits, including filtering patch and dipole antennas. The characteristics of these filtering antennas are compared and discussed.

2.1 Filtering patch antennas

First, a single-polarized filtering patch antenna and a dual-polarized one without extra circuits are introduced.

2.1.1 High-gain single-polarized filtering patch antenna

Fig. 1 illustrates the structure of a single-polarized filtering patch antenna with high-gain radiation performance (Zhang XY et al., 2015). It has two substrates, i.e., sup-substrate (ε_r=2.65 and h_1=2 mm) and sub-substrate (ε_r=2.65 and h_3=3 mm). The stacked and driven patches are printed on the sup- and sub-substrate, respectively. The ground plane is printed on the bottom of the sub-substrate. There are three shorting pins and one U-shaped slot etched on the driven patch for achieving high out-of-band suppression and high roll-off rate near the lower band-edge. The stacked patch is used to enhance the frequency selectivity and gain at the higher frequency band-edge. The filtering patch antenna can cover the Long-Term Evolution (LTE) band (2.3–2.7 GHz). Its average in-band gain reaches 9.7 dBi, and the gain suppression level out of the operating band is more than 21 dB. It is worth mentioning that there are no extra filtering circuits in the antenna. The antenna has three radiation nulls and a flat boresight gain response. The shorting pins and U-shaped slot have little effect on the in-band gain performance.

To analyze the principle of generating the upper-stopband radiation null, a comparison between the gain curves of the patch antennas with and without the

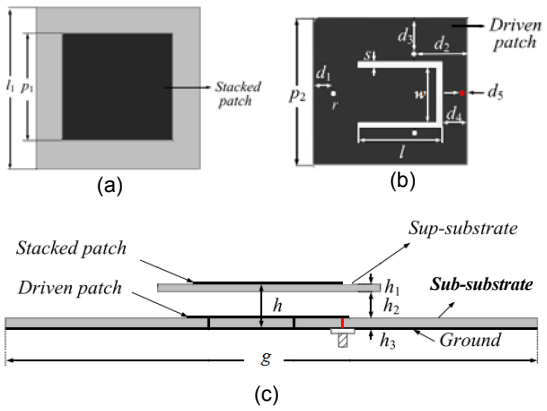

Fig. 1 Geometry of the filtering patch antenna: (a) stacked patch; (b) driven patch; (c) side view

Reprinted from Zhang XY et al. (2015), Copyright 2015, with permission from IEEE

stacked patch is made (Fig. 2a). Both of the patch antennas are fed by a probe and have the same driven patch and ground plane. The antenna with the stacked patch has a wider operating bandwidth and a higher gain. The stacked patch generates a radiation null near the upper edge of the passband. Fig. 2b demonstrates that one radiation null is created at 1.5 GHz near the lower edge of the passband by three shorting pins, and the roll-off performance at the lower edge of the passband can be improved. It is observed in Fig. 2c that a radiation null is generated at 2 GHz by the U-shaped slot. In this way, three radiation nulls at 1.5, 2.0, and 3.1 GHz are generated respectively, resulting in a good filtering radiation response.

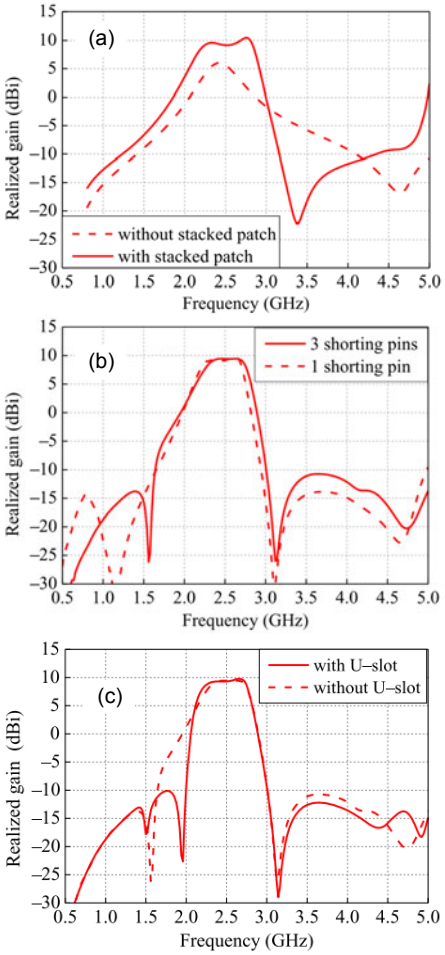

Fig. 2 Realized gain: (a) conventional patch antenna and stacked patch antenna; (b) stacked antenna with one shorting pin and three shorting pins; (c) stacked antenna with and without a U-slot

Reprinted from Zhang XY et al. (2015), Copyright 2015, with permission from IEEE

2.1.2 Dual-polarized filtering patch antenna with high selectivity and low cross polarization

It is difficult to develop a dual-polarized filtering antenna following the above-mentioned antenna design guideline (Zhang XY et al., 2015) since the antenna has an unsymmetrical structure. To avoid this problem, a modified dual-polarized filtering patch antenna was proposed by Duan et al. (2016).

The dual-polarized filtering patch antenna consists of two substrates (Fig. 3). There is a stacked patch on the top of the sup-substrate (ε_r=2.65, 1 mm thickness), the driven patch is printed on the top of the sub-substrate (ε_r=2.65, 1 mm thickness), and the feeding network is printed on the bottom. The bandwidth of the antenna is improved by the air gap between the sup- and sub-substrate. The coupled feeding network is composed of two perpendicularly placed H-shaped microstrip lines. This feeding network can realize a radiation null and achieve good roll-off performance at the edge of the passband. It can also reduce the cross-polarization level and enhance polarization isolation. A square patch in the middle of the driven patch is connected with the H-shaped microstrip line by two vias for port 2, which can enhance polarization isolation. Similar to the above-mentioned design, the stacked patch is used to improve the in-band gain and upper-stopband suppression levels. As shown in Fig. 4, the proposed antenna has an impedance bandwidth of 2.46–2.78 GHz

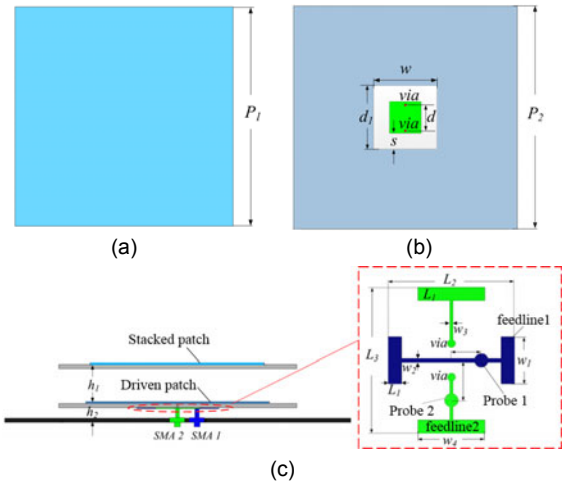

Fig. 3 Geometry of the dual-polarized filtering antenna: (a) stacked patch; (b) driven patch; (c) side view

Reprinted from Duan et al. (2016), Copyright 2016, with permission from IEEE

with a polarization isolation of 35 dB for LTE applications. Its average in-band gain is 9 dBi, and the cross-polarization level is 29 dB. It has a gain suppression level of more than 40 dB in the stopband of 1.71–2.17 GHz (2G and 3G bands).

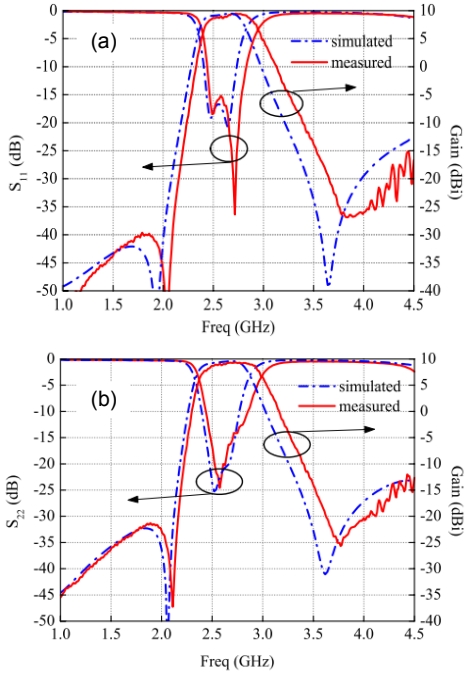

Fig. 4 Reflection coefficients and gain curves: (a) port 1; (b) port 2

Reprinted from Duan et al. (2016), Copyright 2016, with permission from IEEE

To verify the function of the feeding network, a comparison between the gains of antennas with the direct feed and proposed feeding scheme is illustrated in Fig. 5. The proposed feeding circuit can generate a radiation null at 1.9 GHz, while no lower band radiation null is observed in the direct feed case. The frequency of this radiation null can be tuned by varying the length of the feeding line. It is essential that the proposed feeding line has little effect on the flat gain performance within the passband.

2.2 Filtering dipole antennas

We introduce a planar omni-directional filtering dipole antenna and a dual-polarized filtering dipole antenna with broad bandwidth. Since there is no additional filter involved, these two designs are very compact. Their in-band radiation performance has little degradation.

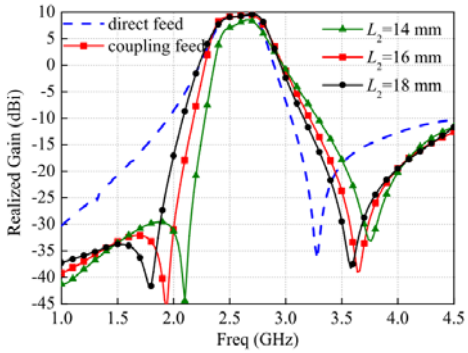

Fig. 5 Simulated gain curves for two different feeding structures

Reprinted from Duan et al. (2016), Copyright 2016, with permission from IEEE

2.2.1 Low-profile planar filtering dipole antennas with omni-directional radiation pattern

Fig. 6 outlines the layout of the filtering dipole antenna (Zhang Y et al., 2018). It is composed of a microstrip-to-slotline-to-microstrip (MTSTM) transition structure as the feeding network and a pair of radiating dipoles. Dipole radiators are connected by a microstrip line, a U-shaped coupling microstrip line, and input feeding lines on the top surface of the substrate. One main slot and two parasitic I-shaped slots are etched on the ground plane on the substrate's bottom surface. The MTSTM transition structure consists of the main slot, an input feeding line, and a microstrip line for connecting the dipoles. The feeding network provides a phase difference of 180° for the dipole radiators, achieving omni-directional radiation. A radiation null at the lower band is generated by the U-shaped coupling microstrip line. The radiation null at the upper band is generated by these two I-shaped slots. As illustrated in Fig. 7, the proposed antenna has an impedance bandwidth (for S_{11}<−10 dB) of 3.82–4.49 GHz (16.1%). The measured gain within the operating band is about 2.5 dBi. The measured level of the out-of-band suppression reaches 15.5 dB in the stopband of 2.0–3.3 GHz and 17.5 dB in the stopband of 5.2–6.0 GHz. The two radiation nulls occur at frequency points of 3.45 and 4.95 GHz, respectively. This implies that the out-of-band radiation is highly suppressed without affecting the passband radiation performance. The curves of S_{11} and boresight gain have good roll-off performance at the higher and lower edges of the passband.

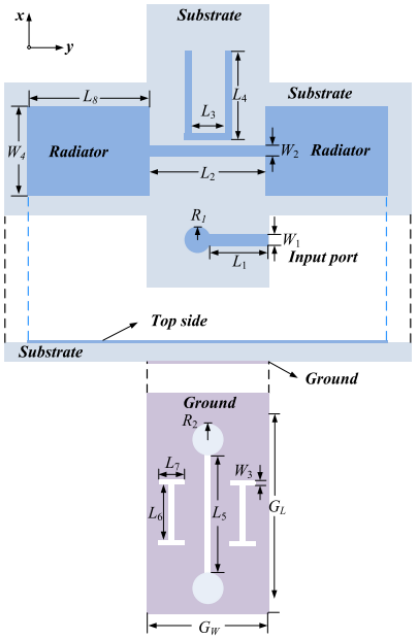

Fig. 6 Configuration of an omni-directional filtering dipole antenna
Reprinted from Zhang Y et al. (2018), Copyright 2018, with permission from IEEE

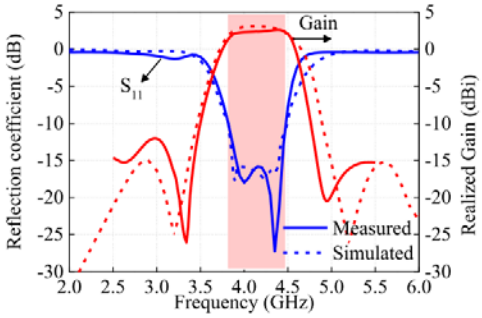

Fig. 7 Measured reflection coefficient and realized gain of the proposed omni-directional filtering dipole antenna
Reprinted from Zhang Y et al. (2018), Copyright 2018, with permission from IEEE

2.2.2 Compact dual-polarized filtering dipole antenna with broad bandwidths and high selectivity

The above-mentioned planar dipole antenna is used in omni-directional radiation applications. To obtain directional radiation patterns, a broadband filtering dipole antenna with dual polarization, applicable for base stations, was proposed with a compact total volume of 50 mm×50 mm×31.8 mm (Ding et al., 2018) (Fig. 8). It consists of two pairs of radiating dipoles fed by baluns, metal reflecting plates,

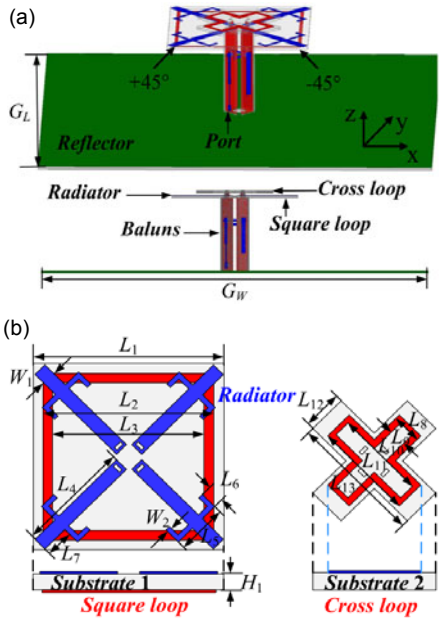

Fig. 8 Configuration of the proposed compact dual-polarized filtering dipole antenna (a) and the radiator and two parasitic loops (b)
Reprinted from Ding et al. (2018), Copyright 2018, with permission from IEEE

and two coupling parasitic loops. Square parasitic and cross-shaped loops are used to generate one radiation null at the lower band and another at the higher band. Simple stubs are extended from the dipole arms to further improve the higher band-edge, roll-off rate, and antenna bandwidth. The operating bandwidth (for voltage standing wave ratio, VSWR<1.5) is 1.66–2.73 GHz (48.7%), as shown in Fig. 9a. The port isolation of the proposed antenna reaches more than 34 dB within the operating bandwidth. The measured in-band gain reaches 8.15 dBi with the stopband gain suppression of more than 17 dB (Fig. 9b). The antenna also has a stable radiation pattern with a half-power beamwidth of about 65.4°.

The operating principle of generating radiation nulls can be explained by the surface current (Fig. 10). For the lower-stopband radiation null, the coupled currents (I_{H1}, I_{H2}, I_{V1}, and I_{V2}) distributed on the larger square loop at 1.45 GHz (stopband) have the opposite direction to the one at 2 GHz (passband). Meanwhile, the flowing direction of the coupled current on the square loop at 1.45 GHz is opposite to that of the current distributed on the dipole. As a result, the radiation of the square-loop coupled current cancels the

dipole, generating a radiation null. For the radiation null at 2 GHz, the currents on the square loop and dipole are in the same direction. Therefore, the operating bandwidth of the antenna can be enhanced due to the contribution of the square loop. Similarly, as shown in Fig. 11, coupled currents on the square loop at 2.7 GHz (passband) have the same direction as the dipole, thereby enhancing the impedance bandwidth. At 2.9 GHz (stopband), the radiation of the dipole is cancelled by both the stub and cross-shaped loop, resulting in better frequency selectivity.

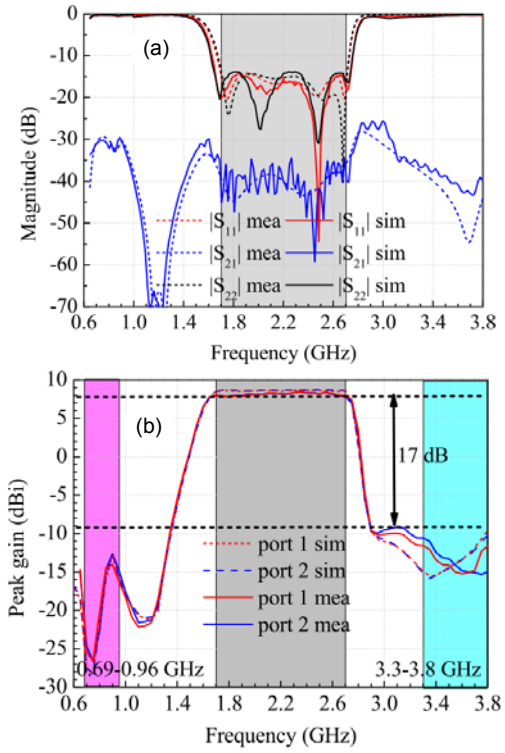

Fig. 9 Measured and simulated S-parameters of the proposed antenna (a) and measured peak gains of the proposed antenna (b)

Reprinted from Ding et al. (2018), Copyright 2018, with permission from IEEE

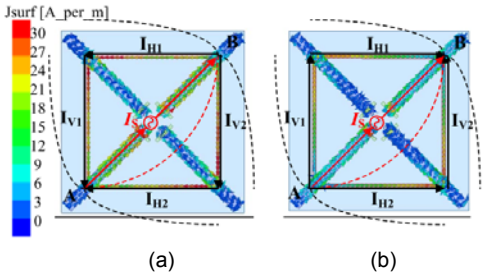

Fig. 10 Simulation current vector distribution: (a) 1.45 GHz (out-of-band); (b) 2 GHz (in-band)

Reprinted from Ding et al. (2018), Copyright 2018, with permission from IEEE

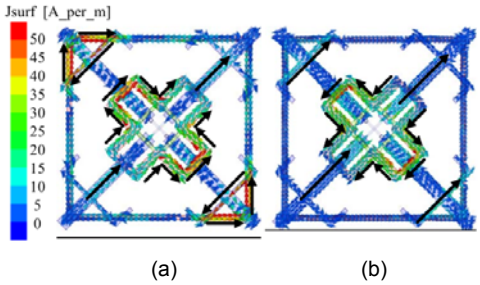

Fig. 11 Simulation current vector distribution: (a) 2.7 GHz (in-band); (b) 2.9 GHz (out-of-band)

Reprinted from Ding et al. (2018), Copyright 2018, with permission from IEEE

3 Dual-band antenna array based on filtering antenna elements

The proposed filtering antennas feature high out-of-band radiation suppression levels without affecting the in-band radiation performance. Therefore, if they are deployed in multi-band antenna array designs instead of traditional non-filtering antennas, the mutual coupling between the subarrays can be effectively reduced. For verification, three dual-band base-station antenna arrays based on filtering antenna elements are proposed in this section.

3.1 Dual-band base station array using filtering antenna elements for mutual coupling suppression

Here, the array is designed based on the two aforementioned filtering antenna elements (Zhang XY et al., 2015) with high in-band radiation efficiency and out-of-band radiation rejection levels. Using the two elements, mutual coupling can be reduced.

Two different filtering antennas operating at different bands are designed (Zhang Y et al., 2016) and placed side by side to form a unit pair (Fig. 12). Elements 1 and 2 are designed for the digital communication system (DCS) (1710–1880 MHz) and wideband code division multiple access (WCDMA) bands (1920–2170 MHz), respectively. For convenience, the two elements are printed on the same substrate with a relative permittivity of 2.65 and a thickness of 3 mm. To stress the advantage of these

filtering antenna elements, a traditional design using two non-filtering antenna elements with the same edge-to-edge spacing is investigated for comparison. The only difference between the filtering and non-filtering antenna unit pairs is that the latter does not have the shorting pins and E-slot.

Fig. 13 shows the comparison results of the two antenna unit pairs. It can be seen that good agreement between the simulation and measurement is achieved, and the filtering antenna unit pair features high isolation of more than 30 dB. The measured impedance bandwidths are 1620–1880 MHz (14.9%) for the DCS band and 1920–2300 MHz (17.9%) for the WCDMA band. In terms of reflection coefficients (S_{11} and S_{22}) and boresight gain responses, good in-band radiating performance and high out-of-band rejection levels are obtained. Meanwhile, both the reflection coefficients and gains have gentle gradients at the edges of the passband, and the isolation is only about 22 dB (Fig. 13b). This means that the improved mutual coupling suppression level in the proposed design is due to the use of filtering antenna elements.

The dual-band filtering antenna array based on the filtering antenna unit pair is shown in Fig. 14. It consists of a large 1×6 subarray for DCS and a small subarray for WCDMA. The distance between the adjacent elements for both subarrays is 130 mm (about $0.78\lambda_0$ in the DCS band and about $0.87\lambda_0$ in the WCDMA band). The two subarrays are placed side by side along the vertical direction with an edge-to-edge spacing of 45 mm. The port-to-port isolation is further improved by an offset between the two arrays in the horizontal direction. Two vertical aluminum reflecting baffles are used to control the 3-dB beamwidth. The size of the complete antenna array including the ground is 835 mm (length)×206 mm (width)×20 mm (height). Compared with the industrial

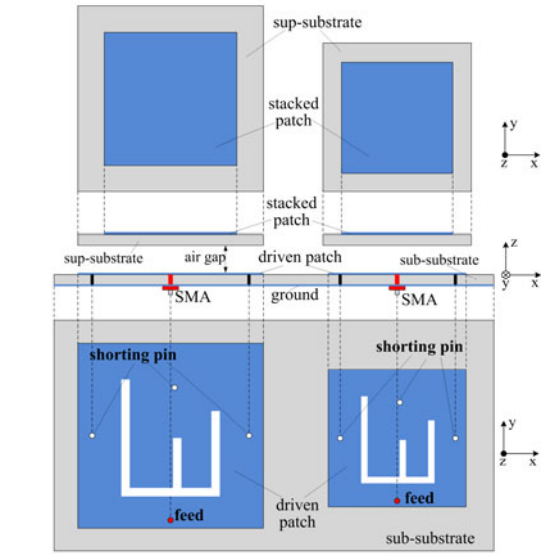

Fig. 12 Configuration of the filtering antenna unit pair
Adapted from Zhang Y et al. (2016), Copyright 2016, with permission from IEEE

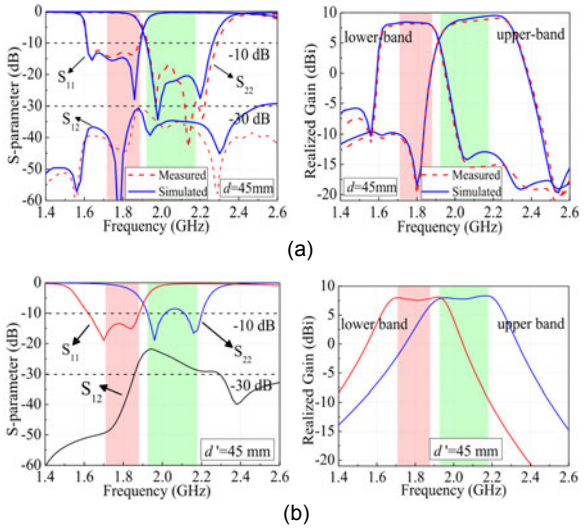

Fig. 13 S-parameters and boresight gains of filtering antenna unit pair (a) and non-filtering antenna unit pair (b)
Reprinted from Zhang Y et al. (2016), Copyright 2016, with permission from IEEE

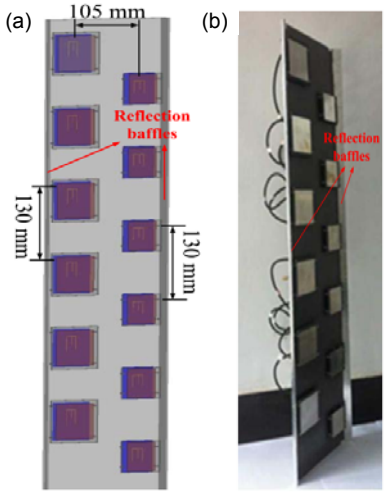

Fig. 14 Proposed dual-band filtering antenna array: (a) top view of the array model; (b) test prototype
Reprinted from Zhang Y et al. (2016), Copyright 2016, with permission from IEEE

products with a width of 290 mm (Andrew Corp., 2007), a size reduction of 28.9% is realized. The feeding network is placed at the back side of the array. As shown in Fig. 15, the feeding network is composed of a planar six-way unequal power divider and six radio frequency (RF) feeding coaxial cables. The feeding has an operating bandwidth of 1710–2170 MHz.

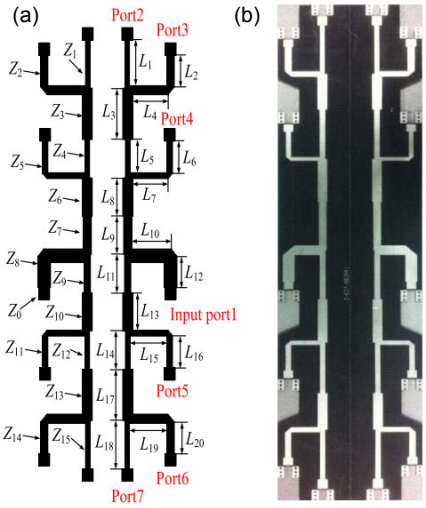

Fig. 15 Dual six-way unequal power dividers: (a) top view of the divider network; (b) prototype
Reprinted from Zhang Y et al. (2016), Copyright 2016, with permission from IEEE

As shown in Fig. 16, the array has impedance bandwidths (for S_{11}<−10 dB) of 1710–1880 MHz for DCS and 1920–2170 MHz for WCDMA, and an isolation of more than 35 dB in the band of 1500–2500 MHz. It has measured gains of about 14.2 dBi in the DCS band and 14.5 dBi in the WCDMA band.

3.2 Compact dual-band dual-polarized interleaved two-beam array with stable radiation pattern based on filtering elements

In this subsection, a dual-band dual-polarized two-beam array is proposed for multi-beam radiation applications. Based on the configuration in Section 2.1.2, the lower-band (LB) and higher-band (HB) elements are designed to operate at 1710–2170 and 2490–2690 MHz for the 3G and LTE applications, respectively. Using the filtering elements, the LB and HB subarrays are interleaved (Zhang XY et al., 2017), as shown in Fig. 17. The two-beam array consists of two 4×4 subarrays, where the larger size is for LB and the smaller size for HB. Based on such a configuration, the array size can be effectively reduced compared to conventional schemes. To maintain good antenna performance with miniaturized array sizes, parameters are chosen for the tradeoff between the S-parameters and radiation performance. It is worth mentioning that in this design, the edge-to-edge spacing between the LB and HB elements is only D_{min}=15 mm ($0.097\lambda_{0L}$ or $0.130\lambda_{0H}$), which is very small. Based on such a compact

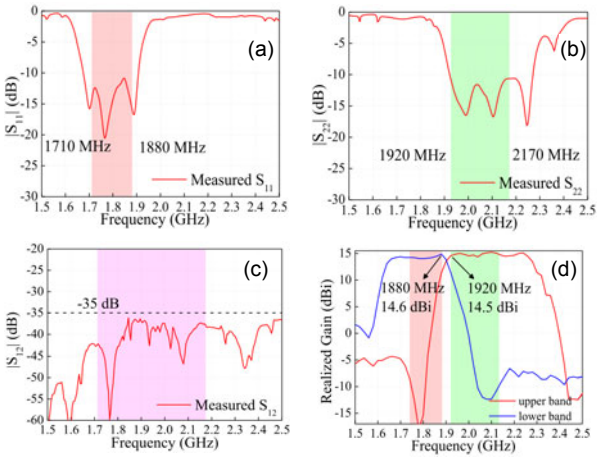

Fig. 16 Measurement results: (a) reflection coefficient of the lower band array; (b) reflection coefficient of the upper band array; (c) isolation parameter $|S_{12}|$; (d) boresight gain of the dual-band filtering antenna array
Reprinted from Zhang Y et al. (2016), Copyright 2016, with permission from IEEE

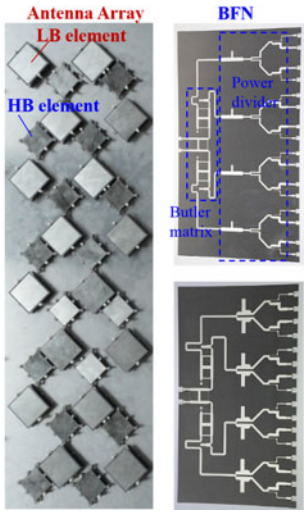

Fig. 17 Prototypes of the antenna array and BFN
Reprinted from Zhang XY et al. (2017), Copyright 2017, with permission from IEEE

configuration, the LB and HB elements are interleaved and the overall size is very small. Two LB and HB beamforming networks (BFNs) are needed for the 4×8 dual-band dual-polarized two-beam array.

Fig. 18 displays the measured realized peak gains from the eight ports. The LB array's peak gains at 2.0 GHz are from 15.3 to 16.4 dBi and the HB array's peak gains at 2.6 GHz are from 14.0 to 15.5 dBi. Its measured normalized radiation patterns in the azimuth plane at the center frequencies of the LB (2.0 GHz) and HB (2.6 GHz) are exhibited in Fig. 19. Two-beam radiation patterns can be observed, and the co-polarization level is at least 14 dB higher than the cross-polarization level in the direction of each beam center. The 10 dB beamwidths range from 107° to 136° with a variation of 29° across the entire operating band. With the azimuth beam centers in the vicinity of ±26°, its azimuth radiation has a 10-dB beamwidth of 120°. Additionally, the cross levels at the junction of both bands are around −10 dB.

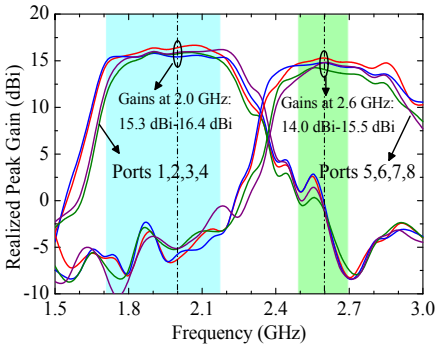

Fig. 18 Measured realized peak gains of the whole 4×8 array

Reprinted from Zhang XY et al. (2017), Copyright 2017, with permission from IEEE

3.3 Dual-band dual-polarized base-station antenna array with a small frequency ratio using embedded filtering elements

In specific base-station applications, the operating frequency bands of the antenna array are close to each other. For such cases, a dual-band ±45° dual-polarized base-station array using embedded filtering elements has been proposed (Duan et al., 2019). The operating frequency bands are 790–862 and 880–960 MHz, indicating a small frequency ratio of 1.1. The LB antenna element is embedded into the HB antenna to achieve a more compact size. The whole array has a width of only 280 mm, which is smaller than the typical industrial products (about 576 mm).

3.3.1 Embedded filtering antenna unit design

Fig. 20 illustrates the structure of the proposed dual-band dual-polarized filtering antenna unit. It is

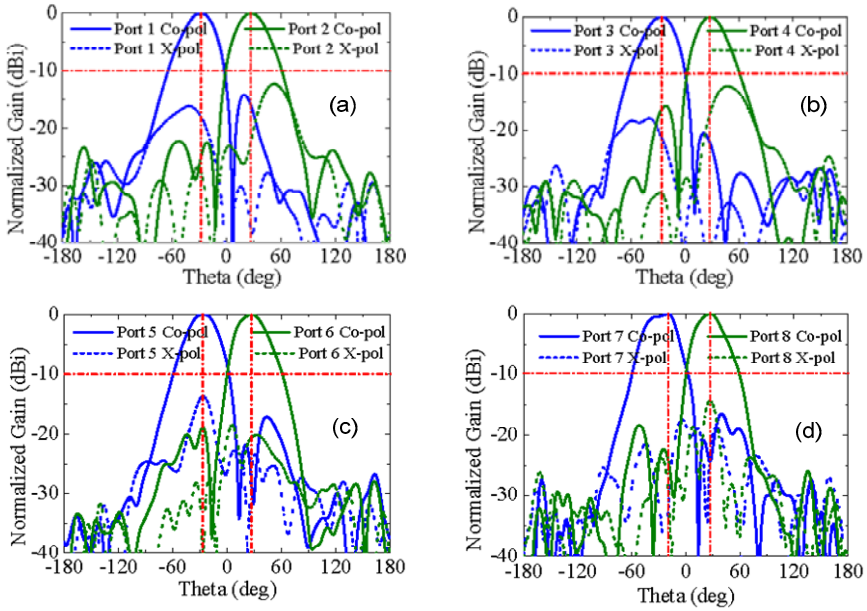

Fig. 19 Measured normalized radiation patterns at center frequencies: (a) port 1/2 excitation at 2.0 GHz; (b) port 3/4 excitation at 2.0 GHz; (c) port 5/6 excitation at 2.6 GHz; (d) port 7/8 excitation at 2.6 GHz

Reprinted from Zhang XY et al. (2017), Copyright 2017, with permission from IEEE

composed of a reflector, a lower-band (790–862 MHz) patch antenna, and four higher-band (880–960 MHz) dipole antennas around the patch antenna. Four metal walls with different heights are placed around the square ground to obtain a high front-to-back ratio and cross-polarization levels. Baseboard 1 is placed below the reflector to fix the patch antenna, and baseboard 2 is used for the dipole antennas. Fig. 21 displays the structure of the lower-band patch antenna, which is similar to the one in Section 2.1.2. The driven patch and feeding network are printed on the top and bottom surfaces of substrate 1, respectively.

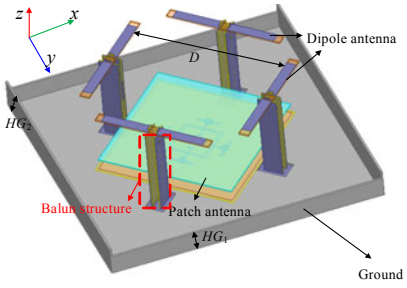

Fig. 20 Three-dimensional configuration of the proposed dual-band dual-polarized filtering antenna unit
Reprinted from Duan et al. (2019), Copyright 2019, with permission from the authors, licensed under CC BY-4.0

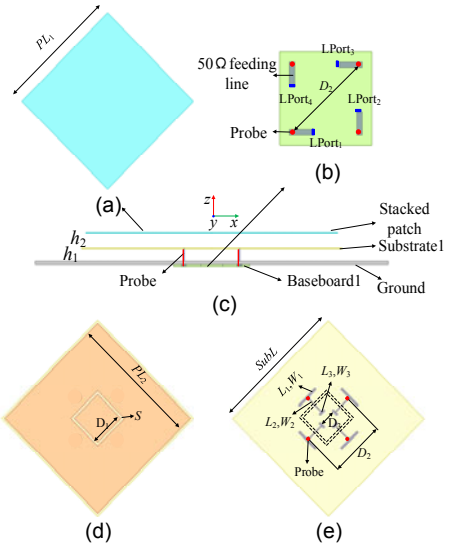

Fig. 21 Configuration of the proposed dual-polarized filtering patch antenna: (a) stacked patch; (b) feeding ports; (c) side view; (d) driven patch; (e) feeding lines
Reprinted from Duan et al. (2019), Copyright 2019, with permission from the authors, licensed under CC BY-4.0

The square stacked patch is above the driven patch. The feeding network of the patch antenna is composed of I-shaped coupled feeding lines on the backside of substrate 1, 50-Ω feeding lines on the backside of baseboard 1, and four probes. Lport_1 and Lport_3 are fed with the same amplitude but different phases for −45° polarization, while LPort_2 and LPort_4 are used for +45° polarization. The isolation between the two polarizations can be enhanced using the differential feeding method.

The upper-band dipole antenna is composed of four symmetrically placed filtering dipole radiators in a square, functioning as a dual-polarized element (Zhang Y et al., 2018). Dipoles 1 and 3 are fed with the same amplitude and phase for the −45° polarization, and dipoles 2 and 4 are for the +45° polarization. The single filtering dipole is made up of a half-wavelength radiating arm, balun, and ground. The balun consists of two substrates (Sub1 and Sub2), which are connected by a metal probe. These two substrates are connected to the dipole arm and baseboard 2 (Fig. 20). The balun feeding network with a bandstop response is on the left side of Sub2. It has a stepped-impedance feeding line with three stub lines (Fig. 22). Stub1 is designed to generate a bandstop response at the lower band-edge. Two other stubs are used for impedance matching.

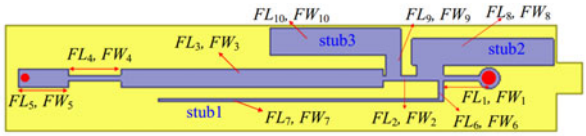

Fig. 22 Configuration of the balun feeding circuit of the proposed dual-polarized filtering dipole antenna
Reprinted from Duan et al. (2019), Copyright 2019, with permission from the authors, licensed under CC BY-4.0

3.3.2 Nine-unit dual-band antenna array design

The structure of the nine-unit antenna array is shown in Fig. 23. The distance between the antenna units is set to 280 mm, i.e., $0.737\lambda_{\mathrm{L}}$ (λ_{L} is the free-space wavelength at 790 MHz). The width of the ground is 280 mm, which is much smaller than that of the industrial products (576 mm). Vertical metal walls are inserted between the antenna units to optimize the front-to-back ratio and cross-polarization levels of the antenna array. To realize high cross-band isolation

between the two embedded elements, the LB patch antenna and HB dipole antenna have bandstop responses at the higher and lower band edges, respectively. The patch antenna array is fed by ports 1 and 2, and the dipole antenna array is fed by ports 3 and 4. Ports 1 and 3 are for −45° polarization, whereas ports 2 and 4 are for +45° polarization.

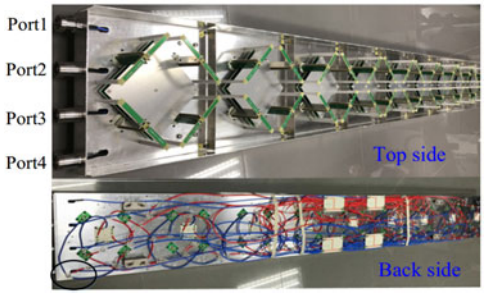

Fig. 23 Photos of the proposed dual-band dual-polarized filtering antenna array with its feeding networks
Reprinted from Duan et al. (2019), Copyright 2019, with permission from the authors, licensed under CC BY-4.0

Fig. 24 demonstrates the measured reflection coefficients and isolations of the proposed dual-band dual-polarized filtering antenna array. The reflection coefficients of lower than −15 dB can be seen in the two operating bands with dual polarization. The in-band polarization isolations are 29 dB for 790–862 MHz and 27.6 dB for 880–960 MHz. Due to the filtering performance of the proposed antenna unit, the isolations between the two bands are 19 dB in the same polarization and 32 dB in the orthogonal polarization. Fig. 25 shows that the simulated gains of the proposed dual-band dual-polarized antenna array in the LB and HB bands are higher than 17.4 and 18 dBi, respectively. The measured gains are 16 and 16.5 dBi for the LB and HB bands, respectively.

4 Conclusions

Several filtering antennas proposed by the authors in the past, including filtering patch and dipole antennas, have been presented in this review. All the proposed antennas feature an innovative conception of eliminating extra filtering circuit, resulting in compact size, simple structure, good in-band radiation performance, and high out-of-band suppression. Three types of dual-band antenna array based on the filtering elements have also been reviewed. Specifically, the dual-polarized antenna array is more compact than the related industry products, and is a good choice for dual-band base-station applications.

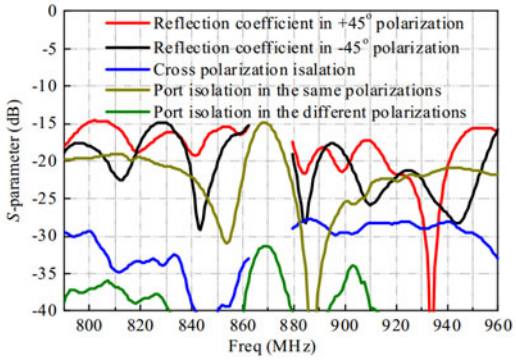

Fig. 24 Measured reflection coefficients and isolations of the proposed filtering antenna array
Reprinted from Duan et al. (2019), Copyright 2019, with permission from the authors, licensed under CC BY-4.0

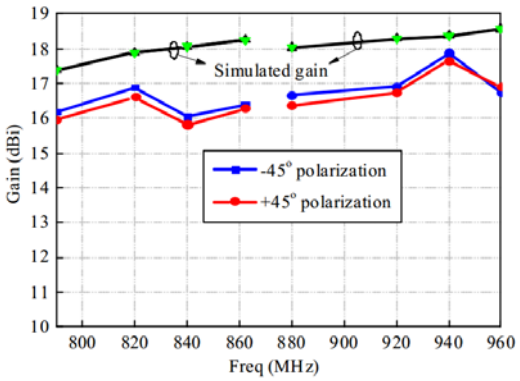

Fig. 25 Gains of the proposed dual-band dual-polarized antenna array
Reprinted from Duan et al. (2019), Copyright 2019, with permission from the authors, licensed under CC BY-4.0

Contributors

Yun-fei CAO wrote and organized the whole manuscript. Yao ZHANG helped write Section 2.1. Xiu-yin ZHANG revised and helped organize the manuscript.

Compliance with ethics guidelines

Yun-fei CAO, Yao ZHANG, and Xiu-yin ZHANG declare that they have no conflict of interest.

References

Andrew Corp., 2007. NNPX306M Datesheet, Hickory, NC, USA.

Chen FC, Hu HT, Li RS, et al., 2017. Design of filtering microstrip antenna array with reduced sidelobe level. *IEEE Trans Antenn Propag*, 65(2):903-908. https://doi.org/10.1109/TAP.2016.2639469

Deng HW, Xu T, Liu F, 2018. Broadband pattern-reconfigurable filtering microstrip antenna with quasi-Yagi structure. *IEEE Antenn Wirel Propag Lett*, 17(7): 1127-1131. https://doi.org/10.1109/LAWP.2018.2825471

Ding CF, Zhang XY, Zhang Y, et al., 2018. Compact broadband dual-polarized filtering dipole antenna with high selectivity for base-station applications. *IEEE Trans Antenn Propag*, 66(11):5747-5756. https://doi.org/10.1109/TAP.2018.2862465

Duan W, Zhang XY, Pan YM, et al., 2016. Dual-polarized filtering antenna with high selectivity and low cross polarization. *IEEE Trans Antenn Propag*, 64(10):4188-4196. https://doi.org/10.1109/TAP.2016.2594818

Duan W, Cao YF, Pan YM, et al., 2019. Compact dual-band dual-polarized base-station antenna array with a small frequency ratio using filtering elements. *IEEE Access*, 7:127800-127808. https://doi.org/10.1109/ACCESS.2019.2939234

Fakharian MM, Rezaei P, Orouji AA, et al., 2016. A wideband and reconfigurable filtering slot antenna. *IEEE Antenn Wirel Propag Lett*, 15:1610-1613. https://doi.org/10.1109/LAWP.2016.2518859

Hsieh CY, Wu CH, Ma TG, 2015. A compact dual-band filtering patch antenna using step impedance resonators. *IEEE Antenn Wirel Propag Lett*, 14:1056-1059. https://doi.org/10.1109/LAWP.2015.2390033

Hu HT, Chen FC, Qian JF, et al., 2017. A differential filtering microstrip antenna array with intrinsic common-mode rejection. *IEEE Trans Antenn Propag*, 65(12):7361-7365. https://doi.org/10.1109/TAP.2017.2764097

Qin PY, Wei F, Guo YJ, 2015. A wideband-to-narrowband tunable antenna using a reconfigurable filter. *IEEE Trans Antenn Propag*, 63(5):2282-2285. https://doi.org/10.1109/TAP.2015.2402295

Sun GH, Wong SW, Zhu L, et al., 2015. A compact printed filtering antenna with good suppression of upper harmonic band. *IEEE Antenn Wirel Propag Lett*, 15:1349-1352. https://doi.org/10.1109/LAWP.2015.2508918

Tang MC, Chen Y, Shi T, et al., 2018. Bandwidth-enhanced, compact, near-field resonant parasitic filtennas with sharp out-of-band suppression. *IEEE Antenn Wirel Propag Lett*, 17(8):1483-1487. https://doi.org/10.1109/LAWP.2018.2850325

Wu JN, Zhao ZQ, Nie ZP, et al., 2013. A broadband unidirectional antenna based on closely spaced loading method. *IEEE Trans Antenn Propag*, 61(1):109-116. https://doi.org/10.1109/TAP.2012.2216492

Wu JN, Zhao ZQ, Nie ZP, et al., 2015. A printed unidirectional antenna with improved upper band-edge selectivity using a parasitic loop. *IEEE Trans Antenn Propag*, 63(4): 1832-1837. https://doi.org/10.1109/TAP.2015.2392112

Zhang XY, Duan W, Pan YM, 2015. High-gain filtering patch antenna without extra circuit. *IEEE Trans Antenn Propag*, 63(12):5883-5888. https://doi.org/10.1109/TAP.2015.2481484

Zhang XY, Xue D, Ye LH, et al., 2017. Compact dual-band dual-polarized interleaved two-beam array with stable radiation pattern based on filtering elements. *IEEE Trans Antenn Propag*, 65(9):4566-4575. https://doi.org/10.1109/TAP.2017.2723914

Zhang Y, Zhang XY, Ye LH, et al., 2016. Dual-band base station array using filtering antenna elements for mutual coupling suppression. *IEEE Trans Antenn Propag*, 64(8):3423-3430. https://doi.org/10.1109/TAP.2016.2574872

Zhang Y, Zhang XY, Pan YM, 2018. Low-profile planar filtering dipole antenna with omnidirectional radiation pattern. *IEEE Trans Antenn Propag*, 66(3):1124-1132. https://doi.org/10.1109/TAP.2018.2790169